Since January 2020 Elsevier has created a COVID-19 resource centre with free information in English and Mandarin on the novel coronavirus COVID-19. The COVID-19 resource centre is hosted on Elsevier Connect, the company's public news and information website.

Biosensors and Bioelectronics 167 (2020) 112465

Contents lists available at ScienceDirect

Biosensors and Bioelectronics

journal homepage: http://www.elsevier.com/locate/bios

A miRNA biosensor based on localized surface plasmon resonance enhanced by surface-bound hybridization chain reaction

Andrea Miti [a], Sophie Thamm [c], Philipp Müller [c], Andrea Csáki [c], Wolfgang Fritzsche [c,**], Giampaolo Zuccheri [a,b,*]

[a] Department of Pharmacy and Biotechnology and Interdepartmental Center for Industrial Research for Life and Health Sciences, University of Bologna, via San Giacomo 11, Bologna, Italy
[b] S3 Center, Institute of Nanoscience of the Italian CNR, Italy
[c] Leibniz Institute of Photonic Technology, Albert-Einstein-Str. 9, 07745, Jena, Germany

ARTICLE INFO

Keywords:
Localized surface plasmon resonance
DNA
microRNA
Hybridization chain reaction
Self-assembly

ABSTRACT

The dysregulation of the concentration of individual circulating microRNAs or small sets of them has been recognized as a marker of disease. For example, an increase of the concentration of circulating miR-17 has been linked to lung cancer and metastatic breast cancer, while its decrease has been found in multiple sclerosis and gastric cancer. Consequently, techniques for the fast, specific and simple quantitation of microRNAs are becoming crucial enablers of early diagnosis and therapeutic follow-up. DNA based biosensors can serve this purpose, overcoming some of the drawbacks of conventional lab-based techniques. Herein, we report a cost-effective, simple and robust biosensor based on localized surface plasmon resonance and hybridization chain reaction. Immobilized gold nanoparticles are used for the detection of miR-17. Specificity of the detection was achieved by the use of hairpin surface-tethered probes and the hybridization chain reaction was used to amplify the detection signal and thus extend the dynamic range of the quantitation. Less than 1 h is needed for the entire procedure that achieved a limit of detection of about 1 pM or 50 amol/measurement, well within the reported useful range for diagnostic applications. We suggest that this technology could be a promising substitute of traditional lab-based techniques for the detection and quantification of miRNAs after these are extracted from diagnostic specimens and their analysis is thus made possible.

1. Introduction

There is an ongoing trend for faster and better performing methods for nucleic acids detection and quantification. Especially when fighting diseases, it is important to have faster and cheaper diagnosis in order to reduce the response time, the stress on patients and the cost of the overall monitoring of large patient cohorts. This is for example the case for cancer screening (World Cancer Report, 2020) or for population testing in rapidly evolving epidemics, as it has recently happened for COVID-19 (Lamb et al., 2020). Very reliable and quick assays are required, in order to detect several markers aiming to return more robust results. MicroRNAs (miRNA) are involved in many cellular processes, such as metabolism, cell growth, and proliferation. MiRNAs are expressed in tissue-specific manners and they are released in bodily fluids such as saliva, urine, and blood, where they are referred to as circulating miRNA (Chandra et al., 2017; Cortez et al., 2011; Hwang and Mendell, 2006; Turchinovich et al., 2011; Vidigal and Ventura, 2015). The concentration of specific sets of miRNA in cells and bodily fluids is altered in pathological conditions, making them a useful class of diagnostic biomarkers for a large number of diseases, if not potentially for all physiological and pathological states (Aushev et al., 2013; Bianchi et al., 2012; Calin and Croce, 2006; Qin et al., 2015; Sethi et al., 2014).

In bodily fluids, miRNAs are not present as simple, soluble and readily detectable RNA, rather they are commonly shuttled around inside stable extracellular lipid-based vesicles. In diagnostics and research, the RNA needs to be extracted from the patient's specimen first, by disassembling such vesicles, before any further analysis. After established molecular biology methods or commercial kits are used to obtain

* Corresponding author. Department of Pharmacy and Biotechnology and Interdepartmental Center for Industrial Research for Life and Health Sciences, University of Bologna, via San Giacomo 11, Bologna, Italy
** Corresponding author.
E-mail address: giampaolo.zuccheri@unibo.it (G. Zuccheri).

https://doi.org/10.1016/j.bios.2020.112465
Received 19 May 2020; Received in revised form 16 July 2020; Accepted 18 July 2020
Available online 1 August 2020

the short RNAs from the specimen, miRNAs are commonly detected and quantified with a choice of lab-based techniques, including qPCR, next generation sequencing or microarrays. Some drawbacks in such lab-based techniques make the detection and quantification of miRNA difficult. The short length of the target sequences, the high sequence homology between miRNAs with different biological roles and their low concentration in biological specimens represent some analytical challenges. Alternative methods and techniques are required in order to make it easier and more reliable to detect and quantitate miRNAs and so advance their uptake as diagnostic biomarkers for disease (Graybill and Bailey, 2016; Tavallaie et al., 2015).

DNA-based biosensors can in principle overcome the complexity and cost of lab-based techniques (Abi et al., 2018; Chao et al., 2016). Of interest for miRNA detection, signal amplification strategies have been devised in order to extend the dynamic range of use of this class of biosensors and facilitate their uptake in diagnostics. Isothermal amplification methods involving DNA have been shown to overcome more complex PCR-based techniques in obtaining quantitative information about the presence of specific nucleic acids (Deng et al., 2017). The hybridization chain reaction (HCR) is an enzyme-free isothermal amplification strategy based on the triggered self-assembly of two DNA hairpins in solution in the presence of a specific target sequence (Dirks and Pierce, 2004). This reaction was proven to be largely adaptable to DNA-based sensing, leading to the enhancement of the sensitivity thanks to the formation of higher molecular weight structures. Promising applications of HCR in biosensing have been reported with various signal detection techniques (Augspurger et al., 2018; Bi et al., 2017). HCR can be exploited in order to accumulate an amount of DNA on a sensing surface: this can then be easily detected, for example, through Surface Plasmon Resonance (SPR) or other label-free techniques (see Table S2). We showed that surface-bound HCR polymerization can be measured with SPR towards the detection of pathogen DNA (Spiga et al., 2014). Localized Surface Plasmon Resonance (LSPR) (Willets and Van Duyne, 2007), a phenomenon involving the interaction between light and metallic nanostructures, allows the realization of simple and small biosensors (Cappi et al., 2013, 2015; Schneider et al., 2013). In LSPR, the energy coupling is observable as a drop in the transmitted light, which yields a peak in the UV–vis absorbance spectrum of the nanoparticles (Jung et al., 1998). A high sensitivity can be achieved by using a simple light source and a spectrophotometer (Chen et al., 2008). LSPR has been proficiently harnessed towards biosensing (Csaki et al., 2018). DNA-based LSPR sensors have been used to detect microbial DNA or RNA and other DNA biomarkers after PCR amplification (Fong and Yung, 2013; Liu et al., 2013; Parab et al., 2010; Soares et al., 2014). Implementations of LSPR for the analysis of miRNA have been previously reported (Joshi et al., 2014; Ki et al., 2019). Ki and coworkers demonstrated that coupling LSPR and HCR provides a gain in sensitivity in the detection (Ki et al., 2019).

We herein propose an innovative and simple biosensor based on HCR and LSPR for the specific detection of miRNAs, and we test it towards the detection of miR-17 sequence. The novelty of the biosensor lies in its simple use of highly-specific hairpin surface probes and the direct connection between target-dependent surface HCR and subsequent LSPR signal generation. The simplicity and effectiveness of this approach make it amenable for diagnostic applications outside the research lab. Mir-17 was chosen as a target to test the biosensor since it is dysregulated in the blood of patients affected by different kinds of cancer and thus it is a promising biomarker for diagnosis and follow-up (Bianchi et al., 2011; Boeri et al., 2011; Dyson et al., 2018; Eichelser et al., 2013; Hesari et al., 2019; Kral et al., 2018; Zeng et al., 2014; Zhang et al., 2019). For example, circulating mir-17 is increased in patients with lung cancer (Momi et al., 2014) and with metastatic breast cancer (Eichelser et al., 2013) or decreased in patients with gastric cancer (Zeng et al., 2014).

2. Material and methods

The LSPR setup employed in this work has been described before (Thamm et al., 2018); a brief description can be found in the Supplementary Information (SI).

The LSPR chips were obtained by immobilizing 80 nm gold nanoparticles on aminopropyl triethoxysilane (APTES)-treated glass slides (see SI, for further experimental details) (Thamm et al., 2018) and they could be stored for up to several days in a dry and clean atmosphere. Immediately before functionalization, the stored chips with the immobilized gold nanoparticles were rinsed with ethanol and ultrapure water, and subsequently subjected to a 1 min UV/Ozone treatment (UV ozone cleaner UVC-1014 NanoBioAnalytics, Berlin, Germany). The thiolated oligonucleotide probe, previously reduced with 20 mM tris (2-carboxyethyl)phosphine) (TCEP) for 1 h in ultrapure water, was adjusted to 2 μM in 0.5 M citrate buffer, pH 6.0, and was deposited on the chip in a controlled-humidity chamber. The probe was then incubated for 18 h at room temperature. After the incubation, the chips were rinsed with citrate buffer and ultrapure water, prior to storage in the running buffer before use (0.75 M NaCl, 75 mM sodium phosphate, pH 6.8). The oligonucleotide-derivatized chips were used within one day of preparation.

Probe-functionalized chips were mounted on the LSPR microfluidic cell and the different target, wash and DNA hairpin solutions were alternatively pumped over the chip surface (as described in the results section) thanks to computer-controlled valve switches. LSPR spectra were recorded every 2 s, the centroid of the LSPR peak was calculated in real-time and displayed (Dahlin et al., 2006). Further details are given in the extended Methods section in the SI.

3. Results and discussion

We obtained the enhancement of a previously developed LSPR nucleic acid biosensor (Thamm et al., 2018; Zopf et al., 2019) by integrating surface HCR on it. This biosensor was reproduced by immobilizing 80 nm spherical gold nanoparticles on glass slides. Gold nanoparticles are chosen for their stability and ease of derivatization. Spherical 80 nm gold nanoparticles area a good compromise as they are stable, commercially available or easy to make in the lab and have a good plasmonic response (Yockell-Lelièvre et al., 2015). They are expected to be sensitive to the neighboring solution environment up to a distance of about 40 nm (Jatschka et al., 2016). Nanoparticles of alternative shapes or larger sizes could yield more sensitive LSPR biosensors but they would be more difficult to source, and more variable in shape, stability and plasmonic properties. The LSPR chips were prepared by adsorbing gold nanoparticles in crowded sub-monolayers. The amount of gold dispersion to use depends on its available concentration and it was optimized under AFM control (see Fig. S1B) so that the large majority of the inter-particle distances was larger than the particle diameter and the plasmonic peak was narrow and reproducible (see SI text for more detail and Fig. S2).

For surface derivatization, the immobilized nanoparticles were exposed to thiolated oligonucleotide probes. Differently from the previously presented versions of this type of biosensor, the nucleic-acid probe for miRNA recognition here was a DNA hairpin oligonucleotide with a 6-nt loop and a 6-nt overhang (see Fig. S10) instead of a linear DNA oligonucleotide. This was chosen in order to maximize the sequence specificity of the interaction with the target, thanks to the energy penalty of the hairpin opening. Consequently, the recognition-dependent HCR reaction is triggered only in the case of complete sequence-specific hairpin unfolding, not simply upon binding of any sequence to the probe (see Scheme 1). The hairpin probe was designed in the context of the guidelines for HCR (Miti and Zuccheri, 2018), and it was merely a thiolated version of one of the two HCR hairpin components. The probe-derivatized chips were passivated with mercaptohexanol (MCH) and salmon sperm DNA. The steps involved in the detection

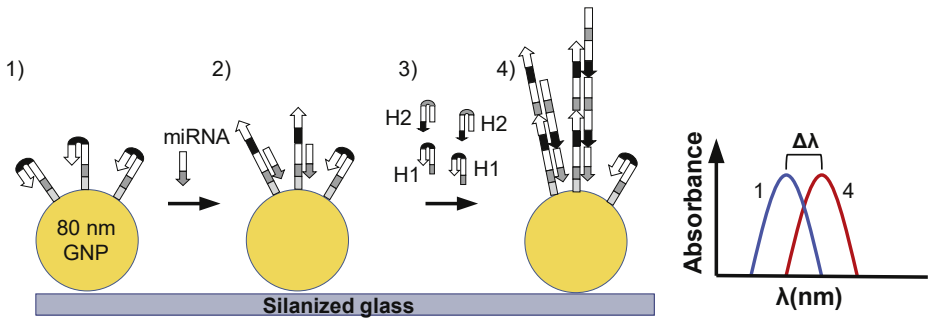

Scheme 1. Scheme of the working principle of the proposed method based on LSPR sensing and Hybridization Chain Reaction (HCR). 1) The probe H1 is immobilized on the gold nanoparticles (GNP) 2) The specific miRNA target is added and it interacts with the specific probe. 3) The mixture of hairpins is added and 4) Hybridization chain reaction takes place on the gold nanoparticles. Each step is monitored using LSPR in real time. The nanoparticles and the DNA molecules are not drawn to scale.

of this enhanced LSPR biosensor are sketched in Scheme 1.

After the glass slides with adsorbed probe-derivatized nanoparticles were prepared, they were mounted in the microfluidic cell and then buffer and DNA oligonucleotides mimicking miR-17 were circulated at 5 μl/min via a computer-controlled peristaltic pump. In order to work in more manageable conditions, our tests were performed with target DNA with the same sequence as the RNA sequences. We assume that our analytical system could be easily tunable to RNA detection at a later stage. An example of the real-time measurement of the centroid of the plasmonic peak is reported in Fig. 1B (together with example plasmonic spectra in Fig. 1A). The binding of miR-17 target led to a progressive shift of the centroid position over time. After flowing the analyte solution, a small amount of washing buffer was circulated in order to allow a differential measurement of the centroid shift in the same solution (refractive index) as the baseline (as indicated by the black bracket in Fig. 1B). After each measurement cycle, the biosensor surface was regenerated by flowing 20 mM HCl (Zopf et al., 2019) and verifying that the baseline centroid location was obtained again. A typical calibration curve of the system response is displayed in Fig. 2 (blue trace) and was obtained from repeated measurements with varying concentrations of miR-17 target sequence, flowed at the same rate for the same time (10 min). For the sake of comparison of the signals, the shifts of the centroids of the plasmonic peaks of each biosensor were normalized to its shift in response to 1 μM analyte. This response to this maximum tested concentration of miR-17 was also considered as a practical index of the quality of the chip in use and a proof of an efficient probe immobilization. The biosensor response to the miR-17 target is linear with the log of the target concentration in the 1 nM-1 μM range (normalized Δcentroid = 0.31*Log(conc./nM) + 0.05 with $R^2 = 0.993$).

The effect of HCR on the calibration curve of the biosensor was tested by performing HCR after the exposure of the biosensor to known concentrations of the specific miR-17 target sequence (Fig. 2, yellow trace). After the non-bound target was removed by washing with running buffer, HCR hairpins were flowed simultaneously through the measurement cell at a constant concentration (0.5 μM for 0.5 h) for all the data points. This operation was performed via a peristaltic pump under computer control so that the overall operator effort was limited to setting up the apparatus. Including HCR made the measurement time 0.5 h longer to allow for the HCR molecular assembly to reach a plateau yield. Globally, the measurement procedure on a specimen took less than 1 h and 50 μl of target solution per measurement point. As shown in Fig. 2, signal gains of about 2-fold for 1 μM and 10 nM target concentration were recorded, while lower signals but due to slightly higher amplification ratios were recorded in the 1 pM–1 nM range. Thereby, we

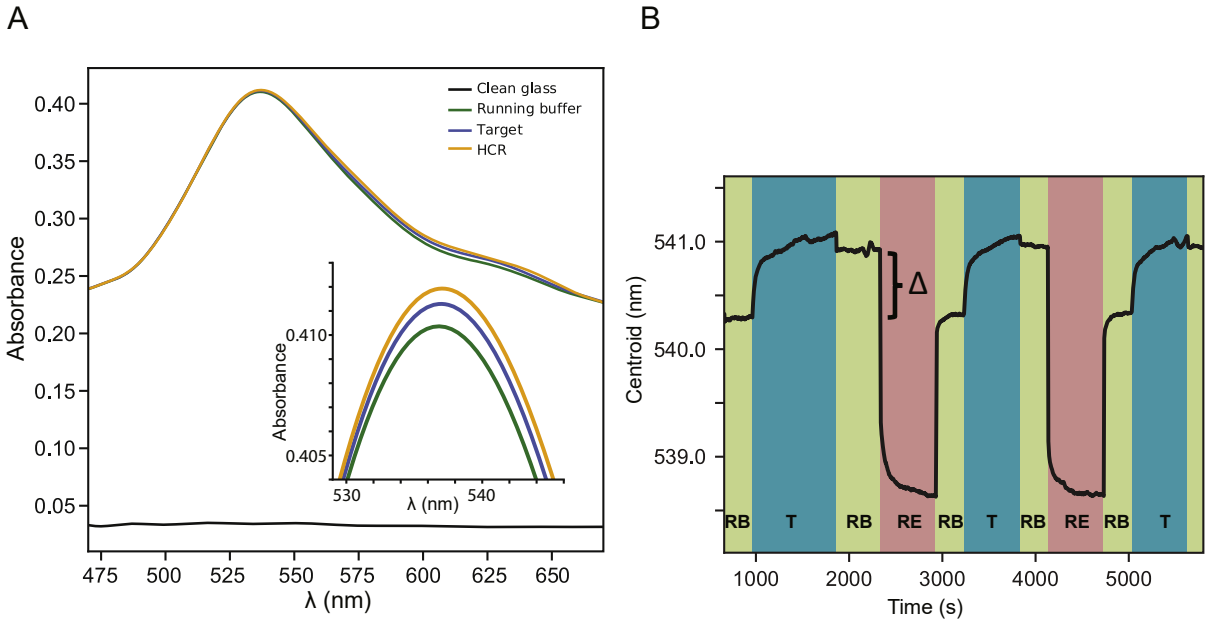

Fig. 1. A) Example spectra for the biosensors before (running buffer) and after exposure to target miR-17 oligonucleotide or full HCR. In the inset, the enlarged detail of the peaks showing the plasmonic shift (the running buffer peak is here centered at 540.6 nm, the target peak at 541.0 nm, the HCR at 541.5 nm). The spectra have been smoothed through polynomial fitting. B) Typical plot of the centroid position over time obtained during the measurement for miR-17 detection in running buffer. On the y-axis is the LSPR centroid wavelength (λ_{LSPR}). The shifts (Δ in the figure) were calculated by taking the difference between the λ_{LSPR} peak position of the plasmonic sensor after and before the injection of miR-17. The concentration of miR-17 here was 1 μM (RB, running buffer; T, target miR-17 oligonucleotide; RE, regeneration solution).

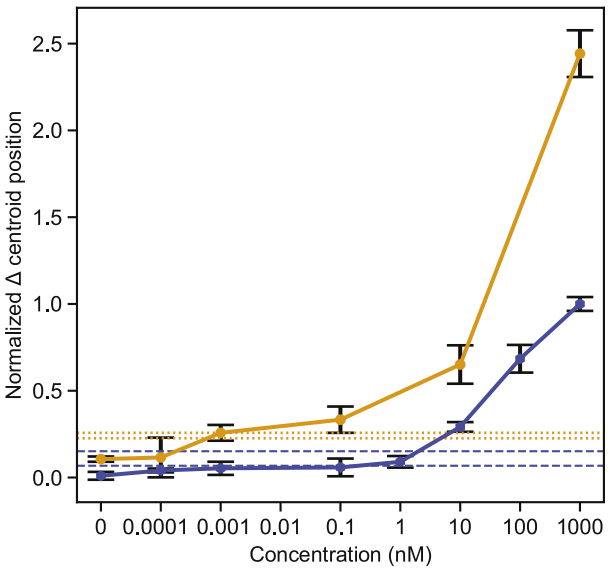

Fig. 2. Calibration curve for the response of the miRNA biosensor, with and without HCR. Different concentrations of target miR-17 in running buffer were flowed in the chamber followed by injection of the mixture of hairpins at 0.5 μM each in running buffer for 30 min. The blue trace represents the calibration curve for the response to the target only, while the yellow trace represents the cumulative response after HCR amplification. The lower and upper dashed horizontal blue lines correspond to the LOD and the LOQ, respectively, for the biosensor response without HCR. The lower and upper dotted yellow horizontal lines represent the LOD and LOQ for the biosensor response with HCR amplification. The bars correspond to the standard deviations (N = 3). Only the first data point below LOD is plotted in the figure for the yellow HCR trace (C = 0.0001 nM), while the corresponding points are plotted for the blue target-only trace as to show the gain in LOD with HCR. See Figs. S5 and S9 for part of the raw data used for this calibration. (For interpretation of the references to colour in this figure legend, the reader is referred to the Web version of this article.)

can conclude that the HCR decreased the LOD down to the pM target concentration range.

The hybridization chain reaction is often affected by some target-less *leakage* (the self-triggered assembly of the monomers) due to the metastable state of the hairpin monomers. The negative control (only buffer instead of target analyte exposed on the probe) shows a very low signal increase when the HCR hairpins are later circulated (Fig. 2). Since the chips were properly passivated (see Fig. S7), this is probably due to some weak leakage that could not be suppressed while designing hairpins for the natural miR-17 sequence. The use of hairpins at the relatively low 0.5 μM concentration stems from the compromise between a reasonable rate of the HCR and low enough leakage.

We showed that it is also possible to reuse the biosensors as to allow for higher productivity/sensor (see Fig. S3): this aspect could be useful towards research bioanalytics or environmental testing, but it is certainly not advisable in diagnostics in order to avoid cross-contaminations.

The Student t-test was performed to confirm that the measurements after HCR are statistically different from those before HCR ($P \leq 0.01$) in the 1 pM-1 μM concentration range. The limit of detection (LOD) was estimated as the lowest (measured) target concentration with a signal higher than the signal of the blank added to 3 times its standard deviation. The limit of quantitation (LOQ) was estimated adding the signal of the blank to 10 times its standard deviation (Alankar and Vipin B, 2011). The LOD for the LSPR biosensor before the amplification step was estimated at 1 nM, with a LOQ of about 10 nM. HCR reduced the LOD and the LOQ to about 1 pM, suggesting an effective advantage of HCR as an amplification method (Fig. 2, LOD and LOQ are the lower and higher horizontal dashed lines, for both HCR-less and HCR-enhanced measurements). These LOD and LOQ values are in the proper range for miRNA detection in bodily fluids, where the concentrations are expected to range from femtomolar to nanomolar (Zouari et al., 2018). As the volume of each target analyte injection was 50 μL, the LSPR biosensor can detect about 50 amol of miRNA. The ability to operate with such small volumes of diluted miRNA solution should make our biosensor method compliant with the available volumes of patient specimens derived from liquid biopsies and the needed sample pre-processing and extraction procedures.

Previously reported LSPR based methods could in some cases reach slightly lower LODs than that herein reported, however they employed much more complicated setups and procedures. Ki et al. reported detecting 2.6 amol in a 200 μL sample, using complex nanostructured LSPR chips in combination with enzymatic substrate precipitation. The analysis time of the miRNA sensing platform, as commented by the authors themselves, was too long for direct assay as a point-of-care (POC) diagnostic tool in clinical application (Ki et al., 2019). Our approach could achieve a similar LOD, and further technical improvements to our biosensor are still possible. The strategy reported by Joshi et al. for miRNA detection yielded a limit of detection of about 30 fM. It requires peculiar gold nanostructures and longer analysis times (Joshi et al., 2014). Moreover, the authors use a linear single-stranded probe and it is not clear if the authors verified that it can distinguish homologous miRNA sequences: a critical issue since diagnostic detection deals with a complex miRNA mix (*vide infra* our tests for non-target sequences). Na et al. presented a LSPR assay using HCR and DNAzyme activity as a double amplification, reaching a limit of detection of about 2 pM in buffer, not far from our findings. Their overall protocol required complex manipulation, transfer of the samples and time-consuming incubations (Na et al., 2018). We can thus state that our proposed biosensor can represent a viable result of simplicity, scalability and performance that should prove useful towards the POC sensing of miRNA of diagnostic interest. Further comparison with the available literature is presented in Table S2.

The specific hairpin monomers H1 and H2 here employed were designed for miR-17 detection (Miti and Zuccheri, 2018). Their self-assembly was first demonstrated by us through experiments in solution (see section S4 in SI). An important issue in microRNA detection is the discrimination between similar sequences. The specificity of the system in solution was verified by testing the detection in the presence of miR-106b, with high sequence homology with miR-17, and in the presence of several other unrelated miRNA sequences (see Figs. S14 and S15).

In order to test for the specificity of the LSPR biosensor detection, miR-21 and miR-106b non-target sequences were used (Fig. 3). miR-21 is another commonly dysregulated miRNA in diseases such as cancer (Wu et al., 2015), while, as mentioned above, miR-106b holds a very close sequence similarity to miR-17 (see Table S3) so it was tested as a possible challenging interferent. The LSPR measurements of the alternative analytes were performed in the same conditions as the miR-17 targets (1 μM conc.) and the results are displayed in Fig. 3 (blue bars). The system designed for detecting miR-17 displays a significantly higher signal (5-fold higher) as a response to miR-17 than to the highly homologous miR-106b and an even higher signal (10-fold) with respect to the same concentration of miR-21, which gave a barely detectable signal. Not only the signal due to the highly homologous miR-106b is much lower than that due to miR-17, but the kinetics of the change in the LSPR signal was also markedly different (see Fig. S4). The Student t-test confirmed that the measurements after HCR are statistically different from those before HCR for miR-17 detection ($P \leq 0.01$) while a statistically significant difference was not confirmed for the non-specific miR-106b and miR-21 (p-values are greater than 0.1).

As also described before, a second biosensor signal was then recorded after performing HCR for miR-17 to test for the extent and specificity of signal amplification. As showed in Fig. 3, HCR led to a significantly higher signal in the case of the specific target (2.5 fold higher). In the case of a non-specific binding, such as for miR-106b and

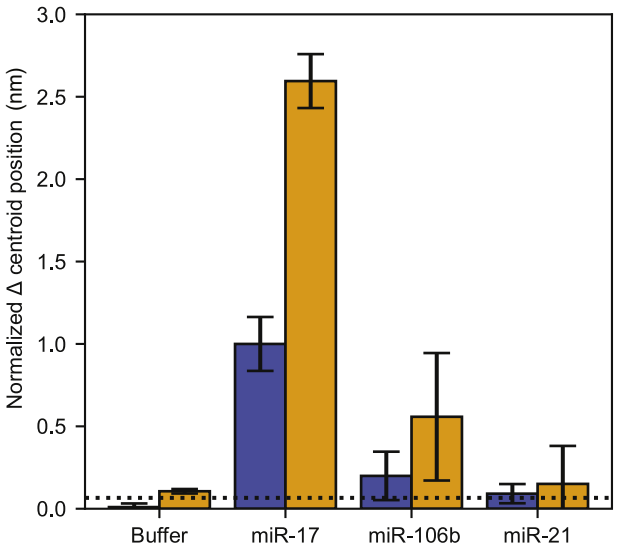

Fig. 3. Test for the specificity of the biosensor: miR-17 probe and hairpins were tested with miR-17 and with highly-homologous miR-106b and with more significantly different miR-21. Normalized average shift in the centroid position are displayed corresponding to the miRNA sequence detection (blue bars) and the overall response performing HCR (orange bars). Error bars correspond to standard deviation (N = 3). The black line corresponds to the LOD (before HCR) as defined in Fig. 1 and in the main text. Error bars correspond to standard deviation (N = 3). (For interpretation of the references to colour in this figure legend, the reader is referred to the Web version of this article.)

miR-21, HCR still amplified the signal, albeit to some lower extent: the specific HCR signal is still about 5-fold higher than the non-specific one from the most homologous miR-106b.

The use of a hairpin surface-probe in the biosensor implies an energy penalty thwarting non-specific binding, due to the stable secondary structure of the hairpin stem that protects at least part of the recognition sequence. This type of probe is widely employed in sensing applications, including strategies involving so-called E-DNA or molecular beacons (Du et al., 2005; Huang et al., 2015; Jiao et al., 2020; Wei et al., 2020). In our case, a non-specific sequence should not be able to unpair the hairpin, while the totally specific complementary sequence induces the switch in the conformation, triggering the HCR self-assembly. The advantages of using a hairpin probe have been confirmed by thermodynamic analysis in NUPACK (Zadeh et al., 2011): a linear single stranded probe for miR-17 would easily interact with miR-106b, while a much lower probability of interaction is found between hairpin H1 and miR-106b. This was confirmed by the experiments in solution that showed a very high specificity in the triggering with miR-17 *vs.* miR-106b (see Fig. S14). The hairpin probe was designed to interact at the 3′ terminus of the miRNA (see Fig. S12): this region has been observed to be more variable in miRNAs, and, in particular, miR-106b misses two bases at the 3' terminus, in addition to a guanine replaced with an adenine in the same region. These differences should impair the formation of the complex, enhancing the specificity. Moreover, a much slower assembly kinetics is expected, as this is strongly dependent on the base pairing at the hairpin toehold, which is reduced for miR-106b.

When performing HCR on the nanoparticle surface, a visible (though not very statistically significant, *vide supra*) HCR enhancement of the LSPR is also measured when testing for the non-specific miR-106b, albeit on a lower signal (Fig. 3). We can hypothesize that the immobilization of the probe on the gold surface could have an effect on the stability of the hairpin: the charge density, and the steric hindrance on the surface of the gold nanoparticles may slightly enhance the switching of H1 to a partially open conformation, more prone to non-specific triggering than the same sets of sequences when tested in solution (see Fig. 3 *vs.* Fig. S14). Local surface defects or chemical inhomogeneities near the probes could possibly lead to the higher signal variability found for this probe. Even if the specificity of the surface-bound hairpin probe was lower than in solution, our biosensor could clearly give a much higher signal with the specific miR-17 target than with miR-106b, the most homologous sequence found in the miRNA databases.

In our experimental set-up, the measurements and the fluidics are fully automated using pumps under the control of a custom-made software. A further obvious development of the sensing strategy and the measurement apparatus could entail the multiplexed HCR and measurement over a small number of miRNA-specific probes. In such envisaged development, the calibration of the system with non-specific miRNAs should allow for the subtraction of cross-over readings and improve the sequence specificity further from what reported here. This development is not expected to require novel technological components. Spherical gold nanoparticles are easily accessible, while light sources and spectrophotometers can be miniaturized allowing the portability and applicability in POC clinical analysis.

4. Conclusions

We herein presented a novel combination of hybridization chain reaction and LSPR-based sensing towards the specific detection of short nucleic acids, such as circulating miRNA. The innovation lies in the combined use of hairpin probes for recognition specificity, and HCR for surface-bound isothermal enzyme-free amplification that directly yields an increased LSPR signal. We showed that our biosensing strategy is amenable to the detection of the diagnostically relevant miR-17 in clinically-relevant quantities and concentrations. Furthermore, the biosensor is robust in the presence of other interfering miRNA sequences, as a mix of miRNAs are expected to be always present in the samples processed from patients' bodily fluids. In our implementation, the full measurement procedure of one specimen can take less than 1 h.

Envisaged further developments of the apparatus fluidics and optical detection can multiplex the detection system as to allow the simultaneous specific and sensitive detection of a panel of diagnostically-relevant miRNA within the same response time in the context of POC diagnostics.

CRediT authorship contribution statement

Andrea Miti: Investigation, Methodology, Formal analysis, Writing - original draft. **Sophie Thamm:** Investigation. **Philipp Müller:** Resources, Software. **Andrea Csáki:** Project administration, Writing - review & editing. **Wolfgang Fritzsche:** Supervision, Writing - review & editing. **Giampaolo Zuccheri:** Supervision, Project administration, Methodology, Formal analysis, Writing - original draft, Writing - review & editing.

Declaration of competing interest

The authors declare that they have no known competing financial interests or personal relationships that could have appeared to influence the work reported in this paper.

Acknowledgements

We thankfully acknowledge Desiree Braun for assistance in the preparation of the sensor chips . This study was funded by DFG (FKZ: FR 1348/31-1), and NanoWater (BMBF, FKZ: 02WIL1521).

Appendix A. Supplementary data

Supplementary data to this article can be found online at https://doi.org/10.1016/j.bios.2020.112465.

References

Abi, A., Mohammadpour, Z., Zuo, X.L., Safavi, A., 2018. Biosens. Bioelectron. 102, 479–489.

Alankar, S., Vipin B, G., 2011. 2, 21-25.

Augspurger, E.E., Rana, M., Yigit, M.V., 2018. ACS Sens. 3, 878–902.

Aushev, V.N., Zborovskaya, I.B., Laktionov, K.K., Girard, N., Cros, M.P., Herceg, Z., Krutovskikh, V., 2013. PloS One 8, 10.

Bi, S., Yue, S.Z., Zhang, S.S., 2017. Chem. Soc. Rev. 46, 4281–4298.

Bianchi, F., Nicassio, F., Marzi, M., Belloni, E., Dall'olio, V., Bernard, L., Pelosi, G., Maisonneuve, P., Veronesi, G., Di Fiore, P.P., 2011. EMBO Mol. Med. 3, 495–503.

Bianchi, F., Nicassio, F., Veronesi, G., Di Fiore, P.P., 2012. Ecancermedicalscience 6, 246.

Boeri, M., Verri, C., Conte, D., Roz, L., Modena, P., Facchinetti, F., Calabro, E., Croce, C. M., Pastorino, U., Sozzi, G., 2011. Proc. Natl. Acad. Sci. U. S. A. 108, 3713–3718.

Calin, G.A., Croce, C.M., 2006. Nat. Rev. Canc. 6, 857–866.

Cappi, G., Accastelli, E., Cantale, V., Rampi, M.A., Benini, L., Guiducci, C., 2013. Sensor. Actuator. B Chem. 176, 225–231.

Cappi, G., Spiga, F.M., Moncada, Y., Ferretti, A., Beyeler, M., Bianchessi, M., Decosterd, L., Buclin, T., Guiducci, C., 2015. Anal. Chem. 87, 5278–5285.

Chandra, S., Vimal, D., Sharma, D., Rai, V., Gupta, S.C., Chowdhuri, D.K., 2017. Life Sci. 185, 8–14.

Chao, J., Zhu, D., Zhang, Y.N., Wang, L.H., Fan, C.H., 2016. Biosens. Bioelectron. 76, 68–79.

Chen, H.J., Kou, X.S., Yang, Z., Ni, W.H., Wang, J.F., 2008. Langmuir 24, 5233–5237.

Cortez, M.A., Bueso-Ramos, C., Ferdin, J., Lopez-Berestein, G., Sood, A.K., Calin, G.A., 2011. Nat. Rev. Clin. Oncol. 8, 467–477.

Csaki, A., Stranik, O., Fritzsche, W., 2018. Expert Rev. Mol. Diagn. 18, 279–296.

Dahlin, A.B., Tegenfeldt, J.O., Hook, F., 2006. Anal. Chem. 78, 4416–4423.

Deng, R.J., Zhang, K.X., Li, J.H., 2017. Accounts Chem. Res. 50, 1059–1068.

Dirks, R.M., Pierce, N.A., 2004. Proc. Natl. Acad. Sci. U. S. A. 101, 15275–15278.

Du, H., Strohsahl, C.M., Camera, J., Miller, B.L., Krauss, T.D., 2005. J. Am. Chem. Soc. 127, 7932–7940.

Dyson, G., Ferran, B., Bolton, S., Craig, D.B., Dombkowski, A., Beebe-Dimmer, J.L., Powell, I.J., Podgorski, I., Heilbrun, L.K., Bock, C.H., 2018. Am. J. Canc. Res. 8, 2088.

Eichelser, C., Flesch-Janys, D., Chang-Claude, J., Pantel, K., Schwarzenbach, H., 2013. Clin. Chem. 59, 1489–1496.

Fong, K.E., Yung, L.Y.L., 2013. Nanoscale 5, 12043–12071.

Graybill, R.M., Bailey, R.C., 2016. Anal. Chem. 88, 431–450.

Hesari, A., Azizian, M., Darabi, H., Nesaei, A., Hosseini, S.A., Salarinia, R., Motaghi, A.A., Ghasemi, F., 2019. J. Cell. Biochem. 120, 7109–7114.

Huang, J.H., Wu, J.Q., Li, Z.G., 2015. Rev. Anal. Chem. 34, 1–27.

Hwang, H.W., Mendell, J.T., 2006. Br. J. Canc. 94, 776–780.

Jatschka, J., Dathe, A., Csáki, A., Fritzsche, W., Stranik, O., 2016. Sens. Bio-Sens. Res. 7, 62–70.

Jiao, J., Li, C., Ning, L.M., Shi, L., Wang, L., Xiang, Y., Li, G.X., 2020. Sensor. Actuator. B Chem. 302.

Joshi, G.K., Deitz-Mcelyea, S., Johnson, M., Mali, S., Korc, M., Sardar, R., 2014. Nano Lett. 14, 6955–6963.

Jung, L.S., Campbell, C.T., Chinowsky, T.M., Mar, M.N., Yee, S.S., 1998. Langmuir 14, 5636–5648.

Ki, J., Lee, H.Y., Son, H.Y., Huh, Y.M., Haam, S., 2019. ACS Appl. Mater. Interfaces 11, 18923–18929.

Kral, J., Korenkova, V., Novosadova, V., Langerova, L., Schneiderova, M., Liska, V., Levy, M., Veskrnova, V., Spicak, J., Opattova, A., Jiraskova, K., Vymetalkova, V., Vodicka, P., Slyskova, J., 2018. Carcinogenesis 39, 1359–1367.

Lamb, L.E., Bartolone, S.N., Ward, E., Chancellor, M.B., 2020. Available at: SSRNL. https://ssrn.com/abstract=3539654. http://doi.org/10.2139/ssrn.3539654.

Liu, P., Yang, X.H., Sun, S., Wang, Q., Wang, K.M., Huang, J., Liu, J.B., He, L.L., 2013. Anal. Chem. 85, 7689–7695.

Miti, A., Zuccheri, G., 2018. Hybridization chain reaction design and biosensor implementation. In: Zuccheri, G. (Ed.), DNA Nanotechnology: Methods and Protocols. Springer New York, New York, NY, pp. 115–135.

Momi, N., Kaur, S., Rachagani, S., Ganti, A.K., Batra, S.K., 2014. Trends Mol. Med. 20, 36–47.

Na, H.K., Wi, J.S., Son, H.Y., Ok, J.G., Huh, Y.M., Lee, T.G., 2018. Biosens. Bioelectron. 113, 39–45.

Parab, H.J., Jung, C., Lee, J.H., Park, H.G., 2010. Biosens. Bioelectron. 26, 667–673.

Qin, X., Xu, H.S., Gong, W.R., Deng, W.B., 2015. Front. Oncol. 4, 7.

Schneider, T., Jahr, N., Jatschka, J., Csaki, A., Stranik, O., Fritzsche, W., 2013. J. Nanoparticle Res. 15.

Sethi, S., Ali, S., Sarkar, F.H., 2014. Clin. Genet. 86, 68–73.

Soares, L., Csaki, A., Jatschka, J., Fritzsche, W., Flores, O., Franco, R., Pereira, E., 2014. Analyst 139, 4964–4973.

Spiga, F.M., Bonyar, A., Ring, B., Onofri, M., Vinelli, A., Santha, H., Guiducci, C., Zuccheri, G., 2014. Biosens. Bioelectron. 54, 102–108.

Tavallaie, R., De Almeida, S.R.M., Gooding, J.J., 2015. Wiley Interdiscipl. Rev. Nanomed. Nanobiotechnol. 7, 580–592.

Thamm, S., Csàki, A., Fritzsche, W., 2018. LSPR detection of nucleic acids on nanoparticle monolayers. In: Zuccheri, G. (Ed.), DNA Nanotechnology: Methods and Protocols. Springer New York, New York, NY, pp. 163–171.

Turchinovich, A., Weiz, L., Langheinz, A., Burwinkel, B., 2011. Nucleic Acids Res. 39, 7223–7233.

Vidigal, J.A., Ventura, A., 2015. Trends Cell Biol. 25, 137–147.

Wei, X.T., Liu, D.W., Zhao, M., Yang, T.T., Fan, Y.P., Chen, W.Q., Liu, P., Li, J.B., Ding, S. J., 2020. Anal. Chim. Acta 1108, 21–27.

Willets, K.A., Van Duyne, R.P., 2007. Annu. Rev. Phys. Chem. 58, 267–297.

World Cancer Report, 2020. In: Wild, C., Weiderpass, E., Stewart, B. (Eds.), World Cancer Report: Cancer Research for Cancer Prevention. International Agency for Research on Cancer (Lyon).

Wu, K.L., Li, L.W., Li, S.Y., 2015. Tumor Biol. 36, 1973–1981.

Yockell-Lelièvre, H., Lussier, F., Masson, J.-F., 2015. J. Phys. Chem. C 119, 28577–28585.

Zadeh, J.N., Steenberg, C.D., Bois, J.S., Wolfe, B.R., Pierce, M.B., Khan, A.R., Dirks, R.M., Pierce, N.A., 2011. J. Comput. Chem. 32, 170–173.

Zeng, Q.H., Jin, C.H., Chen, W.H., Xia, F., Wang, Q., Fan, F., Du, J., Guo, Y.H., Lin, C.W., Yang, K.Y., Li, J.J., Peng, X.W., Li, X.R., Cao, K., 2014. Chin. J. Canc. Res. 26, 711–716.

Zhang, Y., Zhang, Y.M., Yin, Y.H., Li, S.H., 2019. Pathology Research and Practice 215.

Zopf, D., Pittner, A., Dathe, A., Grosse, N., Csaki, A., Arstila, K., Toppari, J.J., Schott, W., Dontsov, D., Uhlrich, G., Fritzsche, W., Stranik, O., 2019. ACS Sens. 4, 335–343.

Zouari, M., Campuzano, S., Pingarron, J.M., Raouafi, N., 2018. ACS Omega 3, 8923–8931.